Simultaneous Measurement of Myocardial Oxygen Consumption and Blood Flow Using [1-Carbon-11]Acetate

Karl T. Sun, Lawrence A. Yeatman, Denis B. Buxton, Kewei Chen, Jay A. Johnson, Sung-Cheng Huang, Klaus F. Kofoed, Susanne Weismueller, Johannes Czernin, Michael E. Phelps and Heinrich R. Schelbert

Division of Nuclear Medicine, Department of Molecular and Medical Pharmacology, Laboratory of Structural Biology and Molecular Medicine and Division of Cardiology, School of Medicine, University of California, Los Angeles, California

[1-Carbon-11]acetate has been used as a tracer for oxidative metabolism with PET. The aim of this study was to validate, in humans, a previously proposed two-compartment model for [1-^{11}C]acetate for the noninvasive measurement of myocardial oxygen consumption (MVO_2) and myocardial blood flow (MBF) with PET. **Methods:** Twelve healthy volunteers were studied with [^{13}N]ammonia, [1-^{11}C]acetate and PET. Myocardial oxygen consumption was invasively determined by the Fick method from arterial and coronary sinus O_2 concentrations and from MBF obtained by [^{13}N]ammonia PET. **Results:** Directly measured MVO_2 ranged from 5.2 to 11.1 ml/100 g/min, and MBF ranged from 0.48 to 0.88 ml/g/min. Oxidative flux through the tricarboxylic acid cycle, reflected by the rate constant k_2, which correlated linearly with measured MVO_2 [$k_2 = 0.0071 + 0.0074(MVO_2)$; $r = 0.74$, s.e.e. = 0.015]. With this correlation, MVO_2 could be estimated from the model-derived k_2 value by $MVO_2 = 135(k_2) - 0.96$. The slope of this relationship was close to that previously obtained in rats and implies that the tricarboxylic acid cycle intermediate metabolite pool sizes are comparable. The net extraction (K_1) of [1-^{11}C]acetate, measured by PET, from blood into myocardium correlated closely with MBF by $K_1 = 0.15 + 0.73(MBF)$ ($r = 0.93$, s.e.e. = 0.033) and, thus, provided noninvasively obtainable measures of blood flow. **Conclusion:** The proposed compartment model for [1-^{11}C]acetate fits the measured kinetics well and, with proper calibration, allows estimation of absolute MVO_2 rather than only an index of oxidative metabolism. Furthermore, [1-^{11}C]acetate-derived estimates of MBF are feasible.

Key Words: PET; myocardial oxygen consumption; myocardial blood flow; [1-carbon-11]acetate

J Nucl Med 1998; 39:272–280

Noninvasive measurement of regional functional processes in the human myocardium is afforded by PET. Because PET records only the concentrations of radioactivity in tissue and their changes over time, the quantification of functional processes hinges on the configuration and validation of tracer kinetic models that appropriately relate the externally observed tissue radioactivity concentrations to the functional process to be studied. [1-Carbon-11]acetate has been used with PET as a tracer for the noninvasive assessment of regional myocardial oxidative metabolism. Initially, an index of oxidative metabolism was obtained to estimate myocardial oxygen consumption (MVO_2) noninvasively by mono- or biexponential fitting the tissue time–activity curve (*1–5*). A more advanced approach using tracer kinetic modeling has been recently proposed in isolated rat hearts and validated in vivo in dogs (*6,7*). This new approach offers several advantages over the conventional approach. It accounts for changes in the distribution of the arterial input function, for spillover of activity from the blood pool to the myocardium and for tracer recirculation (*8,9*). Most importantly, this model-based approach allows the quantification of true myocardial oxidative flux rather than only rates of flux. In addition, it might permit the simultaneous quantification of myocardial blood flow (MBF). It was, therefore, the purpose of this study to examine the validity of this tracer compartment model in humans and to explore the possibility of simultaneous measurements of regional MVO_2 and MBF.

Received Dec. 16, 1996; revision accepted Apr. 15, 1997.

For correspondence or reprints contact: Heinrich R. Schelbert, MD, Department of Molecular and Medical Pharmacology, School of Medicine, University of California, Los Angeles, CA 90095-1735.

MATERIALS AND METHODS

Overall Study Design

All volunteers were admitted to the catheterization laboratory on the morning of the study, where they underwent catheterization of the coronary sinus and of the radial artery for sampling arterial and coronary sinus blood during the PET studies. The volunteers were then moved to the imaging laboratory, where the PET studies were performed. There, a dynamic [^{13}N]ammonia study was performed to measure MBF, followed by a dynamic [1-^{11}C]acetate study to estimate MVO_2. Estimated MVO_2 by PET was compared to directly measured MVO_2, calculated by the Fick method from the oxygen concentrations in arterial and coronary sinus blood and MBF from [^{13}N]ammonia PET.

Study Population

Twelve normal volunteers (nine men and three women; mean age = 26 ± 6 yr), without cardiovascular risk factors or known heart disease, were studied. All volunteers had normal resting electrocardiograms. After the rationale, investigative nature and potential risks of the procedure were explained, each study participant signed an informed consent form approved by the University of California, Los Angeles, Human Subject Protection Committee.

Preparation

The volunteers were premedicated with 5 mg of Diazepam and 50 mg of Benadryl orally, 0.5–1.0 hr before the catheterization of the coronary sinus. After local infiltration of the skin with 2% xylocaine, a 6-F sheath was introduced percutaneously into the right internal jugular vein, and a catheter was advanced to the coronary sinus under fluoroscopic guidance. Heart rate, blood pressure and electrocardiogram (ECG) were monitored continuously during the procedure. After local anesthesia with 2% xylocaine, an arterial catheter was placed into the radial artery using the percutaneous Seldinger technique for the withdrawal of arterial blood samples. While the ECG was monitored continuously, the volunteers were then transported from the cardiac procedure room to the imaging laboratory and positioned in the whole-body positron emission tomograph.

PET

Imaging was performed with a whole-body tomograph (model 931/08-12; CTI-Siemens, Knoxville, TN) with simultaneous acqui-

sition of 15 transaxial images. The tomograph has an intrinsic in-plane spatial resolution of 6.5 mm FWHM, an interplane spacing of 6.7 mm and an axial field of view of 10 cm (*10*). The tomographic images were reconstructed using a Shepp filter with a cutoff frequency of 0.3 Nyquist, resulting in an effective in-plane resolution of 11 mm FWHM.

A rectilinear-type scan was obtained for correct positioning, followed by a 20-min transmission scan with a ^{68}Ge ring source for subsequent correction of photon attenuation.

Regional MBF and oxidative metabolism were assessed with [^{13}N]ammonia and [1-^{11}C]acetate, respectively. An average of 20 mCi of [^{13}N]ammonia or [1-^{11}C]acetate was dissolved in 10 ml of 0.9% saline and injected intravenously with an infusion pump as a bolus spread over 15 sec, followed by a flush of normal saline solution for another 15 sec. The [^{13}N]ammonia image acquisition sequence consisted of 12 frames of 10 sec each, 2 frames of 30 sec, 1 frame of 60 sec and 1 frame of 900 sec for a total imaging time of 19 min. Approximately 45 min later, the [1-^{11}C]acetate study was performed. The image acquisition for [1-^{11}C]acetate was as follows: 12 images of 10 sec each followed 5 images of 60 sec each, 3 images of 120 sec each, 2 images of 300 sec each and 1 image of 300 sec, resulting in a total acquisition time of 33 min. Heart rate, blood pressure and ECG were monitored throughout the study.

Metabolic Measurements

Hemoglobin, hematocrit and blood gases were determined in arterial and coronary sinus blood in all 12 studies at the beginning, middle and end of the [^{13}N]ammonia and the [1-^{11}C]acetate studies. Blood gases were measured with a Corning model 168 blood gas analyzer (Corning Inc., Corning, NY). Serum levels of glucose, lactate and free fatty acids were determined at the same time points during 10 of the 12 [1-^{11}C]acetate studies, as described previously (*11*). Myocardial oxygen consumption (ml/100 g/min) and substrate consumptions were calculated by the Fick principle from the arteriovenous differences across the heart, the hematocrit and hemoglobin concentrations and from MBF, as determined with [^{13}N]ammonia PET (*12*).

Measurements of Carbon-11-Labeled CO_2 and Non-CO_2 Components in Blood

Blood samples (1.0 ml each) from the radial artery were drawn at a rate of every 10 sec during the first 2 min after [1-^{11}C]acetate injection and then at 30-sec intervals for the following 2 min, at 1-min intervals for the next 6 min and every 5 min for a further 20 min. The exact weights of the blood samples were determined by weighing the flasks before and after they were filled with blood. Labeled CO_2 was determined by acidification of 1 ml of the arterial blood samples with 0.5 ml of acetic acid (2 *M*, pH 3.3) in a sealed Erlenmeyer flask. Labeled CO_2 was trapped in a center well filled with 0.3 ml of phenylethylamine (*13*) after shaking for 45 min at room temperature. An aliquot of the remaining ^{11}C activity in the flask, representing non-CO_2 ^{11}C components, was also counted.

Measurement of Amino Acids, Tricarboxylic Acid Cycle Intermediates and Acetate

To determine the concentrations of labeled acetate and its metabolites in arterial blood, seven additional blood samples from the radial artery were taken in 4 of the 12 volunteers at 2, 4, 6, 8, 12, 20 and 30 min after intravenous administration of [1-^{11}C]acetate.

Acetate was separated from amino acid and tricarboxylic acid (TCA) cycle metabolites as described previously (*14*). In brief, whole blood (1 ml) was deproteinized with cold $HClO_4$, neutralized and placed on a combined column of 2 ml of Dowex 1 (formate form) on top of 2 ml of Dowex 50 (H^+ form). The column was washed with 6 ml of water to elute nonionized species and then with 10 ml of 0.25 *M* formic acid, which elutes acetate and ketone bodies, leaving amino acid and TCA cycle metabolites behind. The washes and activity remaining on the column were then determined by counting in a gamma counter with appropriate corrections for physical decay of activity. Acetate trapping on the column previously measured with [1-^{14}C]acetate was 98.5% (recovery washing = 97.3%), and β-hydroxybutyrate trapping was 100% (recovery washing = 75%) (spectrophotometric assay).

PET Image Analysis

The PET image files were reconstructed on a VAX 4000 mainframe computer (Digital Equipment Corporation, Maynard, MA). The images were then transferred to a Macintosh IIfx desktop computer (Apple Computer, Inc., Cupertino, CA) and reoriented into six short-axis cuts (*15*). The reslicing parameters were derived from the last frame of the [^{13}N]ammonia study and from an image frame acquired at approximately 4 min after tracer injection in the [1-^{11}C]acetate study when the myocardium was optimally visualized. The reslicing parameters were then applied to all serially acquired image frames. Three 70° to 90° sectorial regions of interest (ROIs) corresponding to the territories of the three major coronary arteries (left anterior descending and left circumflex and right coronary artery) were assigned to a basal, midventricular and apical short-axis cross-section (*16*). The ROIs were then copied to the first 120 sec (12 frames) of the dynamic [^{13}N]ammonia images and to all 23 frames of the dynamic [1-^{11}C]acetate study. Myocardial time–activity curves were then obtained. Because the invasively measured MVO_2 represents an average value for the entire myocardium, the time–activity curves generated for each of the three coronary territories were also averaged to form a single, average time–activity curve for the left ventricular myocardium in each study. The ^{13}N and ^{11}C activities were corrected for partial volume effects with a recovery coefficient assuming a uniform wall thickness of 1 cm for the left ventricular myocardium (*17,18*).

The arterial input function was derived from a small ROI (25 mm^2) that was centered in the left ventricular blood pool and copied to the serially acquired images in both PET studies. Comparison of the arterial input function by direct arterial blood sampling to the input function derived from a ROI within the left ventricular blood pool on the PET images required a calibration factor, which was obtained as described previously (*19*).

Quantification of Myocardial Blood Flow

Myocardial blood flow was quantified from the arterial input function of [^{13}N]ammonia and the myocardial tissue time–activity curve using a previously validated two-compartment model (*20,21*). The rate pressure product (RPP) in most volunteers increased from the [^{13}N]ammonia to the [1-^{11}C]acetate study. Based on the linear correlation between cardiac workload and flow (*16,22–24*), MBF during the [1-^{11}C]acetate study was extrapolated by using a previously established linear relationship between RPP and MBF in normal volunteers (MBF = 0.0000884*RPP + 0.051) (*25*). Myocardial blood flow during [1-^{11}C]acetate study was estimated by using the cross-point between a line through the data point that represents the measured MBF during the [^{13}N]ammonia study with the slope of 0.0000884 and a perpendicular line to the x-axis through the RPP during the [1-^{11}C]acetate study (Fig. 1). This approach accommodates for changes in cardiac work between studies and ensures a consistent coupling between MBF and RPP, i.e., an increase in RPP results in an increase in MBF, regardless of whether resting flow is below or above the previously found regression line. Such deviations from the regression line may, to some extent, be caused by interindividual differences in the inotropic state of the myocardium, which the RPP accommodates only incompletely. This correction approach thus accounted for

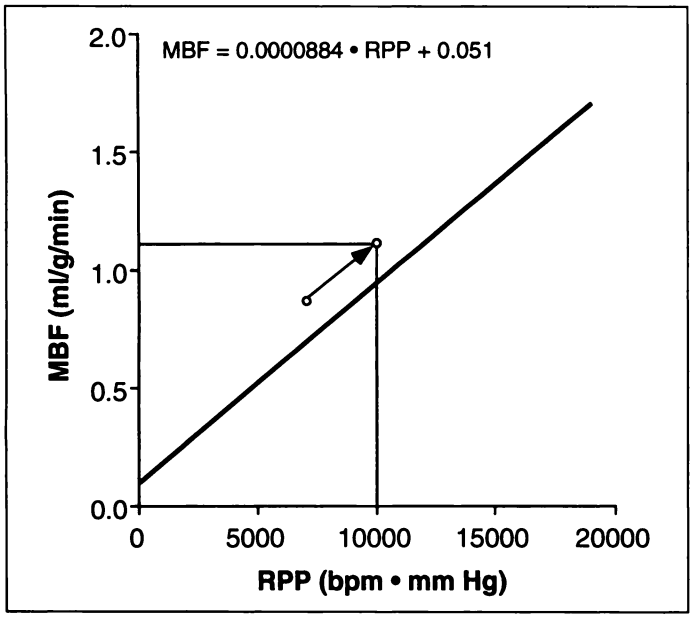

FIGURE 1. Myocardial blood flow at the time of the [1-^{11}C]acetate study was extrapolated from the time of the [^{13}N]ammonia study based on the previously established relationship between RPP as an index of cardiac work and MBF. Myocardial blood flow for a given RPP was estimated by using the cross-point between a line through the measured MBF obtained from the [^{13}N]ammonia study with the slope of 0.0000884 and a perpendicular line through the RPP measured during the [1-^{11}C]acetate scan.

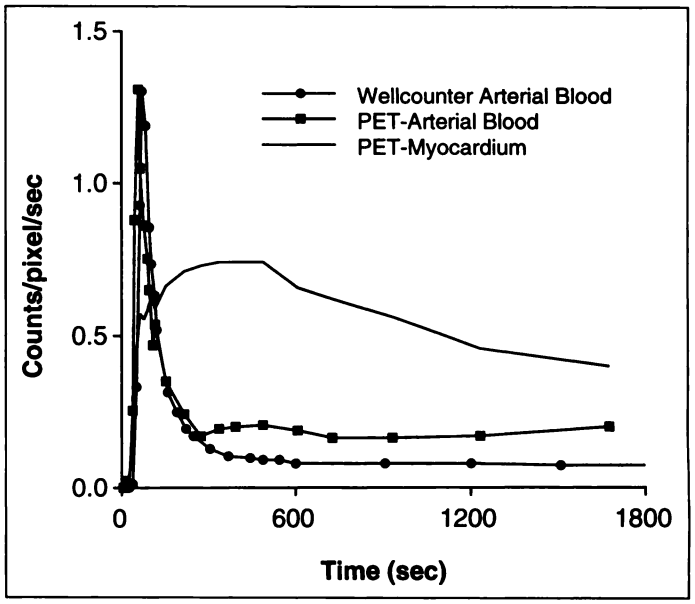

FIGURE 3. Directly (well counter) measured activities in arterial blood (●) and radiotracer concentrations measured with PET in the blood pool (■) and the myocardium (PET myocardium; ——). The blood pool activity measured by PET was consistently higher, due to spillover from myocardium to blood.

interindividual differences in the inotropic state or deviations from the regression line.

Data Analysis

The analyses for mono- and biexponential curve fitting and for model fitting were performed on a Macintosh IIfx desktop computer using a custom-developed toolbox based on the Matlab version 3.5 program (Mathwork Inc., Natick, MA). The tissue time–activity curves obtained from the serially acquired PET images were fitted both biexponentially, beginning with the data point at which the washout phase became linear (k_{bi}), and monoexponentially, using only the initial linear portion of the tissue time–activity curve (k_{mono}) (*2,3,26*). The parts of the time–activity curve that were fitted in this manner were selected by visual inspection.

A two-compartment model that was validated previously in dogs was used in this study (Fig. 2) (*27*). Unlike this earlier study in dogs, in which the curve fitting with the two-compartment model was performed over 5–10 min, here, the tissue time–activity curves

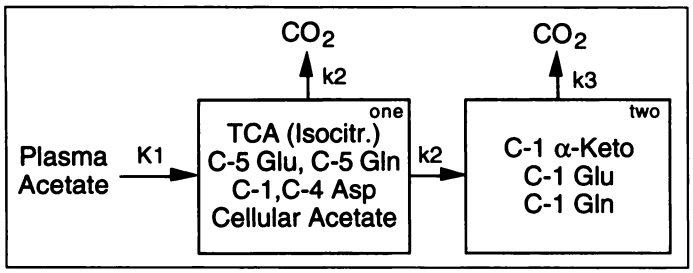

FIGURE 2. Configuration of the two-compartment model for [1-^{11}C]acetate. K_1 denotes the rate of extraction of labeled acetate from the vascular space into the cell, and k_2 describes the rate constants for loss of tracer from pool one and for transfer of tracer from compartment 1 to compartment 2. Compartment 1 represents the metabolite pools of TCA cycle metabolites, mainly isocitrate, glutamate (Glu), glutamine (Gln) and aspartate (Asp) in the carbon 1, 4 and 5 positions (C-1, C-4 and C-5), whereas compartment 2 describes the pool of α-ketoglutarate (α-keto), glutamate and glutamine with the radiolabel in the carbon 1 (C-1) position. k3 represents the rate constant for efflux of CO_2 from compartment 2.

of the present studies were fitted over 15 min. This period was chosen to include the time of the peak [^{11}C]CO_2 efflux, which occurred between 8 and 10 min after tracer injection. Curve fitting over longer time periods did not, as initial studies indicated, yield better or more accurate estimates. The model fitting was performed using a constraint optimization algorithm ("sequential quadratic programming") in the optimization toolbox of Matlab (*28*). Because the compartment model describes the biochemical changes less reliably, very early after tracer injection (negligible concentrations of labeled metabolites and amino acids), data points in the first 2 min were given 20 times less weight. This weighting factor was determined empirically. However, it is noteworthy that the sensitivity of the results to weighting is low, i.e., different weighting did not yield significantly different estimates.

Spillover of activity from blood to myocardium (including the vascular volume of the myocardium) was estimated simultaneously with the rate constants of the two-compartment [1-^{11}C]acetate model, as published previously (*29*). A total of four parameters, i.e., K_1, k_2 and k_3 and the blood-to-myocardium spillover fraction, were estimated in the model fitting.

For the arterial input function of [^{11}C]acetate, the time–activity curve derived from the serially acquired PET images was used. Corrections for contaminations of this curve by radiolabeled metabolites of [1-^{11}C]acetate were made as shown in "Results." In addition, corrections were also required for spillover of activity from the myocardium to the blood pool. As shown in Figure 3, the PET-derived activity concentrations in the blood pool at later times after tracer injection were consistently higher than the activity concentrations in arterial blood measured directly by well counting. The blood pool curve was therefore corrected for spillover of activity from myocardium into the blood pool at later times. The spillover fraction from myocardium to blood was determined as follows: the difference in activity concentrations in the blood pool, as derived from the PET images, and in arterial blood, as measured directly by well counting, was divided by the average myocardial activity concentration. Data obtained at 25–30 min after tracer injection were used for computing this spillover fraction.

The time delay (time shift between measured input and the true, nonobservable one) was set to be 0 as the arterial input function

TABLE 1
Hemodynamic Parameters, Myocardial Oxygen Consumption, Myocardial Blood Flow and Model-Derived k_2

Volunter no.	Heart rate (bpm)		Systolic blood pressure (mm Hg)		Rate pressure product (mmHg · bpm)		MVO_2 (ml/100 g/min)		MBF (ml/g/min)		k_2
	^{13}N	^{11}C	^{13}N	^{11}C	^{13}N	^{11}C	^{13}N	^{11}C	^{13}N	^{11}C	^{11}C
1	73	91	113	127	8,249	11,557	6.4	10.8	0.55	0.75	0.080
2	66	68	113	118	7,458	8,024	7.5	8.1	0.68	0.73	0.048
3	58	68	113	118	6,554	8,024	6.7	8.0	0.52	0.62	0.046
4	59	64	106	119	6,254	7,616	4.9	5.2	0.57	0.68	0.038
5	74	90	108	110	7,992	9,900	9.0	11.0	0.72	0.88	0.071
6	56	68	102	96	5,712	6,528	5.9	6.9	0.57	0.64	0.047
7	45	64	114	121	5,130	7,744	5.3	9.1	0.48	0.70	0.086
8	96	88	112	112	10,752	9,856	9.0	8.4	0.80	0.74	0.060
9	59	63	128	115	7,552	7,245	6.6	7.0	0.67	0.64	0.049
10	54	56	113	109	6,102	6,104	5.8	5.6	0.48	0.48	0.034
11	73	75	106	110	7,738	8,250	6.8	6.5	0.60	0.63	0.047
12	69	83	128	132	8,832	10,956	9.7	11.2	0.70	0.85	0.068
Mean ± s.d.	65 ± 13	73 ± 12*	113 ± 8	116 ± 9	7,360 ± 1,543	8,484 ± 1,712*	7.0 ± 1.5	8.2 ± 2.1†	0.61 ± 0.10	0.70 ± 0.11*	0.056 ± 0.017

bpm = beats per minute.
*$p < 0.01$ vs. ^{13}N
†$p < 0.05$ vs. ^{13}N

was derived from a time–activity curve within the left ventricular cavity (*29*).

Model Estimation of Myocardial Blood Flow

As shown in Figure 2, K_1 in the two-compartment model denotes the net extraction of [1-^{11}C]acetate from the vascular space into the myocardial cell and is estimated by model fitting. Therefore, K_1 as the net extraction is the product of the first-pass extraction fraction of tracer (E) and MBF.

Statistical Analysis

Mean values are given with s.d. Student's t-tests for paired and unpaired data were used, as is appropriate, for comparison. Differences with p values of <0.05 were considered statistically significant. Stepwise regression was used to compare the relationship between arterial substrate levels or consumption and extraction of [1-^{11}C]acetate. The Durbin–Watson test was applied to detect autocorrelated errors (*30*).

RESULTS

Hemodynamic and Metabolic Parameters

Hemodynamic and metabolic findings are summarized in Tables 1 and 2. The mean heart rate increased modestly from the [^{13}N]ammonia studies to the [1-^{11}C]acetate studies ($p < 0.01$), probably because the effects of pharmacological sedation administered before the coronary sinus catheterization were diminishing. Although the systolic blood pressure remained unchanged, the mean RPP increased from the [^{13}N]ammonia studies to the [1-^{11}C]acetate studies ($p < 0.01$). Table 2 lists arterial substrate concentrations and consumption of glucose, lactate and free fatty acid at the time of the [1-^{11}C]acetate studies. No statistically significant correlations between consumption of individual substrates and MVO_2 were noted.

Myocardial Blood Flow and Myocardial Oxygen Consumption

Myocardial blood flow derived from the [^{13}N]ammonia studies averaged 0.61 ± 0.10 ml/g/min. Adjustment of MBFs for the changes in the RPP from the [^{13}N]ammonia to the [1-^{11}C]acetate studies, as described above, resulted in an average blood flow of 0.70 ± 0.11 ml/g/min (Table 1) during the acetate studies. Myocardial oxygen consumption calculated by the Fick principle ranged from 4.9 to 9.7 ml/100 g/min for the [^{13}N]ammonia studies (mean = 7.0 ± 1.5 ml/100 g/min) and from 5.2 to 11.2 ml/100 g/min (mean = 8.2 ± 2.1 ml/100

TABLE 2
Arterial Substrate Concentration and Consumption

Volunteer no.	Arterial concentration			Substrate consumption		
	Glucose (mg/dl)	Lactate (mg/dl)	Free fatty acids (mEq/l)	Glucose (mg/100 g/min)	Lactate (mg/100 g/min)	Free fatty acids (mmol/100 g/min)
1	—	—	—	—	—	—
2	11.6	4.9	0.381	0.71	0.75	0.075
3	103.2	6.6	0.428	1.76	0.86	0.077
4	94.9	6.0	0.751	2.22	0.64	0.082
5	91.7	9.3	0.599	1.44	1.19	0.092
6	—	—	—	—	—	—
7	80.5	5.8	0.477	0.77	0.97	0.068
8	87.1	6.0	0.447	1.67	0.98	0.069
9	86.4	6.6	0.106	1.53	1.33	0.014
10	88.3	6.9	0.336	2.34	0.46	0.037
11	92.7	6.8	0.310	0.99	0.88	0.046
12	85.0	4.4	0.745	1.55	0.58	0.079
Mean ± s.d.	92.3 ± 9.7	6.3 ± 1.3	0.458 ± 0.199	1.50 ± 0.55	0.86 ± 0.27	0.064 ± 0.024

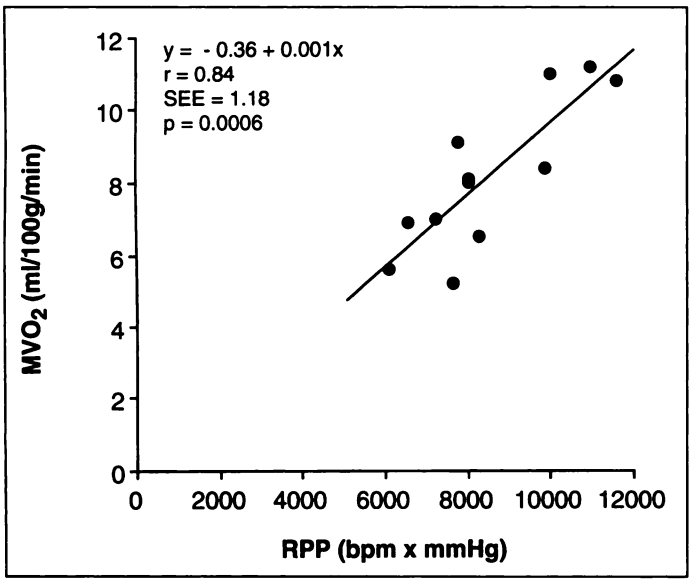

FIGURE 4. Correlation between RPP as an index of cardiac work and invasively measured MVO_2 during the [1-^{11}C]acetate study, determined by the Fick principle.

g/min) for the [1-^{11}C]acetate studies (Table 1). Invasively measured MVO_2 by the Fick principle during the [1-^{11}C]acetate study was correlated linearly with the RPP as an index for cardiac work by $MVO_2 = 0.36 + 0.001(RPP)$ ($r = 0.84$, s.e.e. $= 1.18$, $p = 0.0006$) (Fig. 4). Measured MVO_2 during the [^{13}N]ammonia studies correlated linearly with measured MBF by $MVO_2 = 0.23 + 0.055(MBF)$ ($r = 0.83$, s.e.e. $= 0.06$, $p = 0.0009$). A similar correlation between MVO_2 and MBF was found for the [1-^{11}C]acetate studies [$MVO_2 = 0.34 + 0.043(MBF)$; $r = 0.83$, s.e.e. $= 0.06$, $p = 0.0004$].

Arterial Input Function

The total ^{11}C activity in arterial blood was found to consist of labeled CO_2, acetate, metabolites and TCA cycle intermediates. Thus, the "true" input function of only labeled acetate can be calculated by total ^{11}C activity minus the sum of [^{11}C]CO_2, labeled metabolites and TCA cycle intermediates. The biochemical assays identified three different groups of labeled metabolites of [1-^{11}C]acetate in blood:

1. Labeled CO_2;
2. Nonionized labeled species (such as glucose and cholesterol); and
3. Labeled amino acids and TCA cycle intermediates.

The labeled CO_2 content was measured at the same intervals as was the total blood ^{11}C activity. Thus, the non-CO_2 activity curve can be obtained by subtracting the CO_2 activity from the total measured activity. Table 3 depicts the fractions of [1-^{11}C]acetate in arterial blood (expressed as a percentage of the non-CO_2 portion) in four volunteers and the distribution of the different labeled metabolites of the non-CO_2 fraction over 30 min after intravenous administration of [1-^{11}C]acetate. As the concentration of [1-^{11}C]acetate progressively declined, the fractions of nonionized species, amino acids and TCA-cycle intermediates increased over time. Of note, similar measurements in dogs demonstrated a turnover rate of [1-^{11}C]acetate, which was approximately 1.5–2 times faster than that observed in this study (*27*).

Model Estimates of Regional MVO_2 and MBF

Measured MVO_2 by the Fick method correlated with the model estimated rate constant k_2 linearly by $k_2 = 0.0071 + 0.0074(MVO_2)$ ($r = 0.74$, $p = 0.006$, s.e.e. $= 0.015$). Calculation of mass fluxes requires, in addition to the flux rate, knowledge of the pool sizes of metabolites. When tissue metabolite pool sizes determined previously in isolated perfused rat hearts were used to estimate absolute MVO_2 (in units of ml/100 g/min) by applying the previously established equation (*6*):

$$MVO_2 = 2*k_2*([Glu] + [Asp] + [TCA])*1.5*2,$$
$$\text{or } = 79.2*k_2 \quad \text{Eq. 1}$$

where [Glu], [Asp] and [TCA] describe the pool sizes of glutamate, aspartate and TCA cycle intermediates, respectively, we found that:

$$k_2 = (MVO_2)/79.2 = 0.0126(MVO_2), \quad \text{Eq. 2}$$

which differs only slightly from the relationship found in this study. By rearranging the correlation equation between the measured MVO_2 and the estimated k_2, we find the following relationship between MVO_2 and the model parameter k_2:

$$\text{Estimated } MVO_2 = 135\ k_2 - 0.96. \quad \text{Eq. 3}$$

Using this equation with the k_2 data obtained in this study, the estimated MVO_2 was shown, in Figure 5 and as described below, to have a unity slope against the directly measured MVO_2:

$$\text{Estimated } MVO_2 = 0.019 + 1.008\ MVO_2, r = 0.74, \text{ s.e.e.}$$
$$= 1.98,\ p = 0.006. \quad \text{Eq. 4}$$

The variability of the MVO_2 thus estimated, as compared to that of the directly measured MVO_2, is clearly shown in Figure 5.

The model-derived parameter K_1, which represents the net extraction of [1-^{11}C]acetate from the vascular space into the cell, correlated closely and linearly with estimated MBF by $K_1 = 0.15 + 0.73(MBF)$ ($r = 0.93$, $p < 0.0001$, s.e.e. $= 0.033$) (Fig. 6). The values of MBF in this study, ranging from 0.48 to 0.88 ml/g/min, are similar to those obtained previously in young normal volunteers (*31*). The relatively tight fit of the data with the regression line indicates that, over the flow range studied, the first-pass extraction fraction depends mostly on blood flow. The slope of 0.73 implies a systematic underestimation of true flows by the [1-^{11}C]acetate model, presumably as a consequence of the first-pass extraction fractions being less than unity.

Myocardial Oxygen Consumption and Clearance of Carbon-11 Activity

As shown in Figure 7, k_{bi} and k_{mono}, obtained by bi- and monoexponential curve fitting, respectively, correlated signifi-

TABLE 3
Metabolite Fractions in Arterial Blood*

Time (min)	CO_2 (%)	Acetate (%)	TCA and AA (%)	Nonionic species (%)
2	6.8 ± 1.2	85.8 ± 0.6	4.9 ± 1.7	1.3 ± 1.2
4	16.8 ± 5.4	58.0 ± 3.5	12.7 ± 3.5	2.5 ± 0.8
6	4.74 ± 4.2	33.7 ± 6.2	14.3 ± 4.6	4.6 ± 1.6
8	48.3 ± 4.6	27.7 ± 4.2	17.7 ± 3.1	6.3 ± 1.3
10	60.7 ± 5.4	18.4 ± 2.8	17.3 ± 2.3	5.6 ± 1.0
15	60.9 ± 5.9	14.9 ± 2.0	16.9 ± 2.2	7.0 ± 0.7
20	59.0 ± 4.8	13.9 ± 1.4	18.8 ± 2.2	8.4 ± 0.5
30	62.5 ± 5.8	8.9 ± 1.7	18.3 ± 2.1	10.4 ± 2.5

TCA = TCA cycle intermediates; AA = amino acids.
*Numbers represent percentage of measured total activity in arterial blood obtained by a well counter.

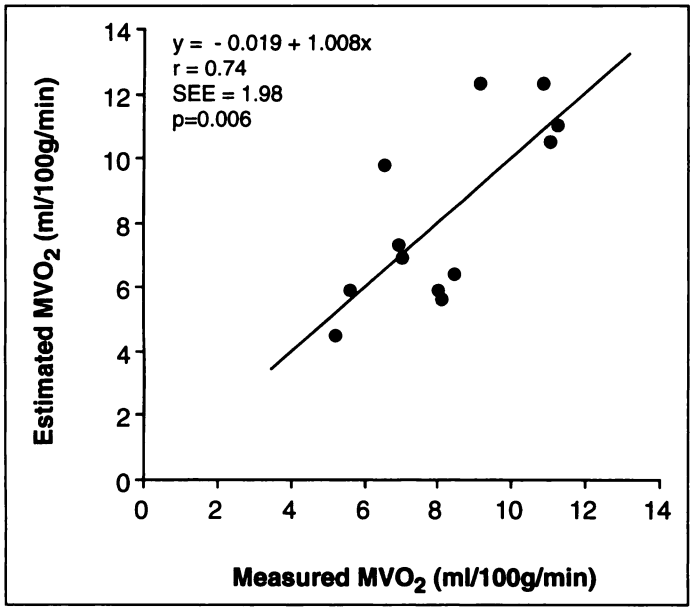

FIGURE 5. Correlation between measured MVO_2 and estimated MVO_2 using the empirically derived relationship between MVO_2 and k_2. Estimated MVO_2 = [(79.2*k_2) − 0.52]/0.59.

cantly to invasively measured MVO_2. The regression lines between k_{bi} and MVO_2 and between k_{mono} and MVO_2 were similar; the intercepts did not differ statistically from 0 ($p > 0.05$).

DISCUSSION

The results of this study demonstrate that a simplified two-compartment model for [1-^{11}C]acetate can be used to derive noninvasively accurate estimates of absolute MVO_2 and MBF. Although the previously used approach with mono- or biexponential curve fitting for determining rate constants of oxidative metabolism has proven useful, the new model approach offers several advantages. The compartment model:

1. Potentially yields absolute values of regional MVO_2 rather than only indices of oxidative metabolism;
2. Accounts for changing shapes of the arterial input function, as shown previously by computer simulations, so that the estimation can be performed automatically and less subjectively (*8*); and
3. Provides simultaneous estimates of MBF.

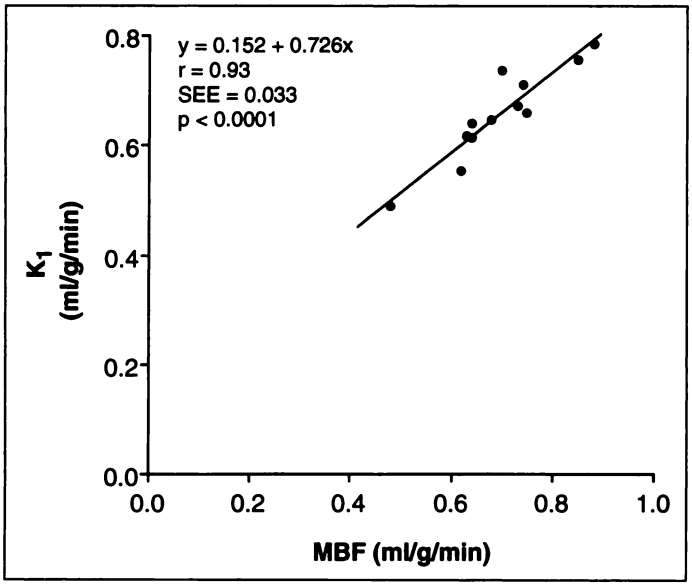

FIGURE 6. Correlation between MBF and the net extraction K_1 of [1-^{11}C]acetate. Note the linear correlation between both parameters over the flow range from 0.5 to 1.0 ml/g/min.

Measurements of Oxygen Consumption

As demonstrated, estimates of MVO_2 in absolute units are possible, but they depend on adequate correction of the PET derived arterial input function for spillover of activity and for contamination by metabolites and on relatively constant distribution volumes for the radiotracer and its metabolites or knowledge of the amount of substrate available (i.e., tissue metabolite pool sizes) for oxidation through the TCA cycle. First, determination of the true arterial tracer input function requires direct measurements of [1-^{11}C]acetate in serial arterial blood samples. Although the radiolabeled acetate is the major component of the input function early after tracer administration, other labeled compounds or metabolites, for example, amino acids, TCA cycle intermediates and CO_2, contribute later, after administration, to the input function. Measurements of these metabolites are essential for accurate estimations of MBF and MVO_2. Determined in 4 of our 12 volunteers in this study, metabolite concentrations varied relatively little between individuals, as indicated by coefficients of variation in the range of about 10%–15% (Table 3). This suggests the possibility of either using a normal database or a correction constant derived from a few measurements of metabolite corrections so that serial blood sampling and blood assays may not always be necessary. Additionally, because the spillover from myocardium to the blood pool (ranging from 5%–20% in the current studies) toward the tail end of the time–activity curve is large, the spillover-corrected PET-left ventricle time–activity curve was used. Lack of corrections for this spillover would have resulted in a systematic overestimation of the rate constant k_2 and, thus, of MVO_2 because of a falsely high arterial input function. This then emphasizes again the need for direct measurements of the arterial input function from either arterial or "arterialized" venous blood samples (*32*).

The spillover fraction can then be determined from directly measured and PET derived arterial tracer activity concentrations. On the other hand, more recently developed analytical approaches such as factor analysis might allow extraction of blood-pool activities with markedly lesser degrees of spillover contamination (*33*). Second, data on metabolite pool sizes in humans myocardium were not available and were difficult to obtain. However, it is important to note that the model-estimated rate constant k_2 was found to be correlated linearly with invasively measured MVO_2. This finding appears to be consistent with earlier observations in isolated rat hearts that metabolite pool sizes in myocardium remain fairly constant over the range of MVO_2 measurements (*6*). This then affords estimates of MVO_2, as indicated above, by rearrangement of the equation for the correlation between true and estimated MVO_2.

The kinetics of a tracer in the myocardium depend on the shape of its arterial input function, which, in turn, depends on the rate of tracer injection, cardiac chamber volumes and/or cardiac output. Monoexponential fitting of the myocardial time–activity curve and, thus, determination of the tissue clearance slope of [1-^{11}C]acetate activity for a given MVO_2, can significantly be affected by the shape of the arterial input function. Input-dependent changes of k_{mono} might, thus, be misinterpreted as true changes in MVO_2 (*8*). Furthermore, monoexponential curve fitting relies on the correct selection of the data points on the time–activity curve. The curve analysis approach is, therefore, observer-dependent and, at times, limited, especially when time–activity curves contain substantial

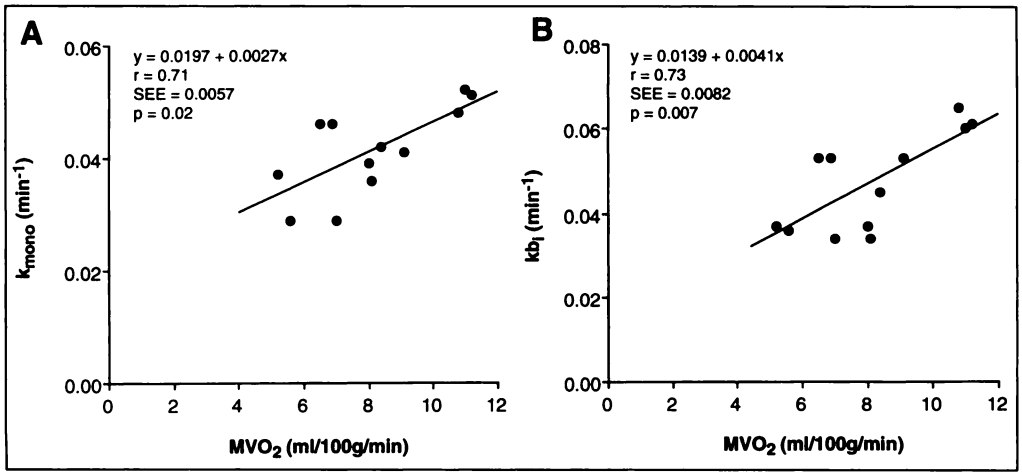

FIGURE 7. Correlation between directly measured MVO_2 and k_{mono} and k_{bi}, respectively. The correlation between k_{bi} and MVO_2 was better than the correlation between k_{mono} and MVO_2.

data noise. Here, k_{bi} derived from biexponential curve fitting and the model-derived rate constant k_2 correlated equally well with measured MVO_2, whereas the correlation between k_{mono} and MVO_2 was less good. This finding is in agreement with earlier observations in canine myocardium where the correlation between MVO_2 and k_{mono} was found to be poorer than that between MVO_2 and k_{bi} (*2*). The good correlation between MVO2 and k_{bi} indicates that k_{bi} could also be used as a good indicator of MVO2 over the range studied. However, using model fitting has many advantages over the biexponential fit, such as:

1. Biexponential fit requires more subjective selection of the time interval for fitting that could vary from study to study.
2. Model fitting results are expected to be more valid over a wider range of physiological conditions. In other words, when the study is expanded to studies in patients, the advantage of the model fitting results is expected to become more apparent.
3. Variation in the shape of the blood time–activity curve (the input function) is properly accounted for by the model, whereas biexponential fitting is more sensitive to this variation. Although the input function can also be incorporated into the biexponential model (by convolving the input function with the biexponential function), the fitting will not be a simple linear fit in the semilogarithmic domain anymore, and it loses its simple computation advantage.
4. The use of model fitting provides, besides MVO_2, additional information on MBF, as shown in Figure 7 and discussed below.

Measurements of Myocardial Blood Flow

Although [1-^{11}C]acetate has been proposed previously as a flow tracer because of its relatively high first-pass extraction fraction, it has not been routinely used for the quantification of MBF (*24,34–36*). Previous studies in dogs demonstrated how the variable first-pass extraction fractions for a given flow precluded accurate flow estimates (*3,7*). Different from dogs however, the first-pass extraction fraction of [1-^{11}C]acetate was found to vary less in humans, and the extraction fractions in normal humans are larger than those in dogs (*7*). In other words, the extraction of [1-^{11}C]acetate from plasma to tissue in humans is not as limiting as it is in dogs. Therefore, the net extraction of [1-^{11}C]acetate from the vascular space into the cell (model parameter K_1) correlated closely and linearly to MBF over a flow range from 0.5 to 1.0 ml/g/min, with relatively little scatter of the data about the regression line. This observation is consistent with data of previous human studies and suggests more accurate estimates of MBF in humans than in dogs (*35,37*). The reason for the large variation of the extraction of [1-^{11}C]acetate in dogs compared to humans remains unclear. Acetate is known to share a common monocarboxylate carrier with lactate and pyruvate for exchange across the sarcolemmal membrane (*38*). The current study, however, failed to reveal a correlation between substrate consumption or substrate levels (glucose, lactate and free fatty acids) and extraction of [1-^{11}C]acetate.

As demonstrated in this study, K_1 is correlated linearly with blood flow, at least over the physiologic range of blood flow at rest. The slope of 0.73 implies a systematic underestimation, most likely because the first-pass extraction fraction is less than unity. Values for K_1 can, however, be corrected from the regression equation describing the correlation between K_1 and MBF.

Study Limitations

There are several limitations to this study. Foremost is the lack of data on the tissue metabolite pool sizes in humans, which would allow direct estimates of MVO_2. To obtain these data would require myocardial biopsies in vivo and labor-intensive analyses, which are difficult to perform and difficult to justify in normal volunteers. However, the linear correlation between k_2 and measured MVO_2 over a wide range, as has also been observed in isolated rat hearts and in vivo dogs, indicates that estimates of MVO_2 can, in fact, be obtained by assuming that the sum of the metabolite concentrations remains fairly constant under different conditions and over a wide range of MVO_2. This has been previously shown in isolated perfused rat hearts (*6*).

Another limitation is the lack of direct MBF measurements during the [1-^{11}C]acetate studies, which was complicated further by a significant increase in the RPP between the [^{13}N]ammonia and the [1-^{11}C]acetate study. This increase most likely resulted from a lessening of the pharmacological sedation induced before coronary sinus catheterization with Diazepam and Benadryl. The extrapolation used a previously established correlation between the RPP and blood flow. It is realized that changes in the RPP are accompanied by proportionate changes in blood flow, and yet the RPP as an index of cardiac work or the approximations of blood flow in the study does not fully accommodate changes in the contractile state (*16,22–24*). The extrapolation approach attempted to preserve the deviation of the flow value from the regression line by using the same y-intercept for the extrapolated as for the measured flow value. Other extrapolation methods, such as the use of different slopes,

may have also been feasible. Given the modest change in RPP, however, it appears that the differences between various extrapolation approaches would have been very small. Moreover, the observed close correlation between K_1 and extrapolated MBF confirms the validity of the correction. Had no corrections been made for the changes in RPP between the two studies (i.e., if MBF of the [^{13}N]ammonia was used), the correlation between the RPP during the [1-^{11}C]acetate studies and MBF would have been insignificant ($p = 0.12$ versus 0.002 for RPP-adjusted MBF). Although additional studies under different conditions (beta-blocker, dipyridamole and dobutamine) would have been desirable to increase the range of MBF and MVO_2, the values found in this study nevertheless represent the physiological range in humans under resting conditions (*16,39*).

Third, no studies were performed in patients with ischemic heart disease or poor left ventricular function. Only normal volunteers with presumably homogeneously distributed rates of oxygen consumption were studied because the invasively measured MVO_2 represents a global rather than a regional value. It is possible that regional estimates of MVO_2 in patients may be affected by differences in tissue metabolite pool sizes due to factors such as altered metabolism in abnormal tissue or medical treatment. Also, the influence of different input shapes or noisy studies, which occur more often in patients with poor left ventricular function, was not explored. Validation of the tracer compartment model in such patients would have been rather complex because it would have required invasive measurements of regional MVO_2 with measurements of local arteriovenous blood O_2 concentrations.

CONCLUSION

Accurate noninvasive simultaneous estimations of absolute MVO_2 and MBF in humans are possible with [1-^{11}C]acetate and a simple compartment model using PET. The compartment model tested in this study can account for changes in the input function and allows an automated analysis of studies in comparison to the conventional approach with mono- or biexponential curve fitting, which are more subjective. Simultaneous measurements of MVO_2 and MBF can provide additional information on, for example, ischemically compromised myocardium. In patients after an acute myocardial infarction, oxygen consumption may not strictly follow blood flow (*40*). Disparities between blood flow and oxygen metabolism may contain prognostic information. Also, as described in another study in early postinfarction patients, the blood flow–MVO_2 relationship may not be linear, but rather, it may be piecewise, which appears to be consistent with compensatory increases in the extraction of oxygen in response to decreases in blood flow (*41*). The described model approach offers measurements of both blood flow and oxygen consumption with a single tracer injection, thus lowering radiation burden to the patient, reducing scanner time and cost while enhancing the clinically useful information.

ACKNOWLEDGMENTS

This study was performed for the U.S. Department of Energy by the University of California under Contract DE-FC03-87ER60615. This work was supported in part by the director of energy research, Office of Health and Environmental Research (Washington, DC), by Research Grants HL 29845 and HL 33177, by the National Institutes of Health (Bethesda, MD) and by an Investigative Group Award by the Greater Los Angeles affiliate of the American Heart Association (Los Angeles, CA). We thank Ron Sumida, Lawrence Pang, Francine Aguilar, Der-Jenn Liu, Sumon Wongpyia, Anh Nguyen, Dr. Paul Natterson, Dr. David DeLurgio, Dr. Anthony Steimle, Dr. Gregg Fonarow and the staff of the medical cyclotron and adult catheterization laboratory at the University of California (Los Angeles, CA) for technical assistance; Deborah Dorsey, MN, for recruiting the volunteers; Diane Martin for preparing the illustrations; and Eileen Rosenfeld for her assistance in preparing this manuscript.

REFERENCES

1. Buxton DB, Schwaiger M, Nguyen A, Phelps ME, Schelbert HR. Radiolabeled acetate as a tracer of myocardial tricarboxylic acid cycle flux. *Circ Res* 1988;63:628–634.
2. Armbrecht JJ, Buxton DB, Brunken RC, Phelps ME, Schelbert HR. Regional myocardial oxygen consumption determined noninvasively in humans with [1-^{11}C] acetate and dynamic positron tomography. *Circulation* 1989;80:863–872.
3. Armbrecht JJ, Buxton DB, Schelbert HR. Validation of [1-^{11}C]acetate as a tracer for noninvasive assessment of oxidative metabolism with positron emission tomography in normal, ischemic, post-ischemic and hyperemic canine myocardium. *Circulation* 1990;81:1594–1605.
4. Brown MA, Myears DW, Bergmann SR. Noninvasive assessment of canine myocardial oxidative metabolism with ^{11}C-acetate and positron emission tomography. *J Am Coll Cardiol* 1988;12:1054–1063.
5. Brown MA, Myears DW, Bergmann SR. Validity of estimates of myocardial oxidative metabolism with carbon-11 acetate and positron emission tomography despite altered patterns of substrate utilization. *J Nucl Med* 1989;30:187–193.
6. Ng CK, Huang SC, Schelbert HR, Buxton DB. Validation of a model for [1-^{11}C] acetate as a tracer of cardiac oxidative metabolism. *Am J Physiol* 1994;266:H1304–H1315.
7. Sun KT, Chen K, Huang SC, et al. A workable compartmental model for simultaneous measurement of myocardial oxygen consumption using C-11 acetate [Abstract]. *J Nucl Med* 1993;34:4P.
8. Chen K, Sun KT, Buxton DB, Hansen HW, Schelbert HR, Huang SC. The effect of plasma time activity curve shape on estimates of myocardial oxygen consumption rate with C-11 acetate studies [Abstract]. *J Nucl Med* 1993;34:50P.
9. Buck A, Wolpers H, Hutchins G, et al. Effect of carbon-11-acetate recirculation on estimates of myocardial oxygen consumption by PET. *J Nucl Med* 1991;32:1950–1957.
10. Spinks TJ, Guzzardi R, Bellina CR. Performance characteristics of a whole-body positron tomograph. *J Nucl Med* 1988;29:1833–1841.
11. Buxton DB, Schwaiger M, Vaghaiwalla Mody F, et al. Regional abnormality of oxygen consumption in reperfused myocardium assessed with [1-^{11}C] acetate and positron emission tomography. *Am J Cardiac Imaging* 1989;3:276–287.
12. Fick A. Ueber die Messung des Blutquantums. In: *Den Herzventrikeln, Verhandlungen der physikalisch-medizinischen*. Würzburg: Gesellschaft; 1870:16.
13. Buffington CK, De Buysere MS, Olson MS. Studies on the regulation of the branched chain a-keto acid dehydrogenase in the perfused rat heart. *J Biol Chem* 1979;254:10453–10458.
14. Randle PJ, England PJ, Denton RM. Control of the tricarboxylate cycle and its interaction with glycolysis during acetate utilization in rat hearts. *Biochem J* 1970;117:677–695.
15. Kuhle W, Porenta G, Huang S-C, Phelps M, Schelbert H. Issues in the quantitation of reoriented cardiac PET images. *J Nucl Med* 1992;33:1235–1242.
16. Czernin J, Müller P, Kim A, et al. Myocardial flow reserve declines with age because of higher cardiac work at rest. [Abstract] *J Nucl Med* 1992;33:836.
17. Hoffman EJ, Huang SC, Phelps ME. Quantitation in positron emission computed tomography. *J Comput Assist Tomogr* 1979;3:299–308.
18. Ratib O, Phelps ME, Huang SC, Henze E, Selin CE, Schelbert HR. Positron tomography with deoxyglucose for estimating local myocardial glucose metabolism. *J Nucl Med* 1982;23:577–586.
19. Phelps ME, Huang SC, Hoffman EJ, Selin C, Sokoloff L, Kuhl DE. Tomographic measurement of local cerebral glucose metabolic rate in humans with (F-18) 2-fluoro-2-deoxy-D-glucose: validation of method. *Ann Neurol* 1979;6:371–388.
20. Smith G, Huang S, Nienaber C, Krivokapich J, Schwaiger M, Schelbert H. Noninvasive quantification of regional myocardial blood flow with N-13 ammonia and dynamic PET [Abstract]. *J Nucl Med* 1988;29:A-950.
21. Kuhle W, Porenta G, Huang S-C, et al. Quantification of regional myocardial blood flow using ^{13}N-ammonia and reoriented dynamic positron emission tomographic imaging. *Circulation* 1992;86:1004–1017.
22. Kitamura K, Jorgensen CR, Gobel FL, Taylor HL, Wang Y. Hemodynamic correlates of myocardial oxygen consumption during upright exercise. *J Appl Physiol* 1972;32:516–522.
23. Baller D, Bretschneider HJ, Hellige G. Validity of myocardial oxygen consumption parameters. *Clin Cardiol* 1979;2:317–327.
24. Krivokapich J, Huang S, Schelbert H. Assessment of the effects of dobutamine on myocardial blood flow and oxidative metabolism in normal human subjects using nitrogen-13 ammonia and carbon-11 acetate. *Am J Cardiol* 1993;71:1351–1356.
25. Sun K, Czernin J, Krivokapich J, et al. Effects of dobutamine stimulation on myocardial blood flow, glucose metabolism and wall motion in PET mismatch regions [Abstract]. *J Am Coll Cardiol* 1994;23:117A.
26. Buxton DB, Nienaber CA, Luxen A, et al. Noninvasive quantitation of regional myocardial oxygen consumption in vivo with [1-^{11}C] acetate and dynamic positron emission tomography. *Circulation* 1989;79:134–142.
27. Sun K, Chen K, Huang S-C, et al. Compartment model for measuring myocardial oxygen consumption using [1-^{11}C] acetate. *J Nucl Med* 1997;38:459–466.
28. Landaw E, Distefano JI. Multiexponential, multicompartmental and noncompartmental modeling. II. Data analysis and statistical considerations. *Am J Physiol* 1984;246:R665–R677.
29. Meyer E. Simultaneous correction for tracer arrival delay and dispersion in CBF

measurements by the $H_2{}^{15}O$ autoradiographic method and dynamic PET. *J Nucl Med* 1989;30:1069–1078.
30. Neter J., Wasserman W, Kutner MH. Applied linear statistical models: regression, analysis of variance and experimental designs., 3rd ed, 1990. Homewood, IL: Irwin, 1181.
31. Czernin J, Muller P, Chan S, et al. Influence of age and hemodynamics on myocardial blood flow and flow reserve. *Circulation* 1993;88:62–69.
32. Weinberg IN, Huang SC, Hoffman EJ, et al. Validation of PET-acquired functions for cardiac studies. *J Nucl Med* 1988;29:241–247.
33. Wu H, Huang S, Allada V, et al. Derivation of input function from FDG-PET studies in small hearts. *J Nucl Med* 1996;37:1717–1722.
34. Gropler RJ, Siegel BA, Geltman EM. Myocardial uptake of carbon-11-acetate as an indirect estimate of regional myocardial blood flow. *J Nucl Med* 1991;32:245–251.
35. Chan S, Brunken R, Phelps M, Schelbert H. Use of the metabolic tracer carbon-11-acetate for evaluation of regional myocardial perfusion. *J Nucl Med* 1991;32:665–672.
36. Böttcher M, DiCarli M, Brunken RC, Czernin J, Sun K, Schelbert HR. Myocardial blood flow measurements using PET and C-11 acetate: a comparison to N-13 ammonia in patients with severe coronary artery disease. [Abstract] *Circulation* 1994;90:I-447.
37. Porenta G, Cherry S, Brunken R, Kuhle W, Schelbert H. Combined dynamic and gated C-11 acetate PET imaging provides estimates of myocardial oxygen extraction and wall tension [Abstract]. *J Am Coll Cardiol* 1991;17:380A.
38. Mann G, Zlokovic B, Yudilevich D. Evidence for a lactate transport system in the sarcolemmal membrane of the perfused rabbit heart: kinetics of unidirectional influx, carrier specificity and effects of glucagon. *Biochim Biophys Acta* 1985;819:241–248.
39. Holmberg S, Serzysko W, Varnauskas E. Coronary circulation during heavy exercise in control subjects and patients with coronary heart disease. *Acta Med Scand* 1971;190:465–480.
40. Hicks R, Melon P, Kalff V, et al. Metabolic imaging by positron emission tomography early after myocardial infarction as a predictor of recovery of myocardial function after reperfusion. *J Nucl Cardiol* 1994;1:124–137.
41. Czernin J, Porenta G, Brunken R, et al. Regional blood flow, oxidative metabolism and glucose utilization in patients with recent myocardial infarction. *Circulation* 1993;88: 885–895.

(continued from page 9A)

FIRST IMPRESSIONS
Urine Contamination Simulating Spinal Metastases

Figure 1.

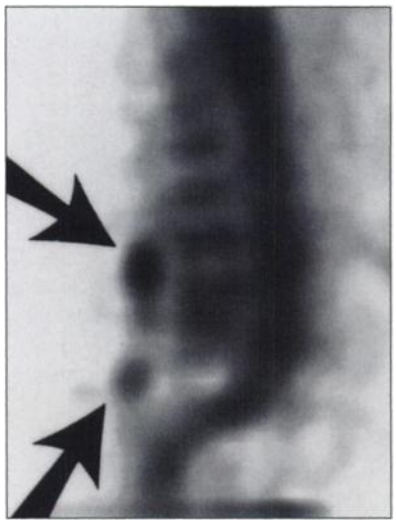

Figure 2.

PURPOSE
A 61-yr-old woman with lung cancer status post radiation therapy presents with new-onset back pain. New contiguous spread of tumor to the right hemivertebrae of T3–T5 was confirmed by SPECT imaging. Additional moderately intense uptake in the posterior elements of the upper lumbar spine on planar imaging suggests distant metastases (Fig. 1). SPECT imaging demonstrates skin contamination on the sagittal projection (Fig. 2), which disappears on postwash planar images.

TRACER
Technetium-99m-MDP (21.8 mCi)

ROUTE OF ADMINISTRATION
Intravenous

TIME AFTER INJECTION
3 hr

INSTRUMENTATION
GE Maxxus gamma camera

CONTRIBUTORS
Erica A. Guzalo, Elizabeth Oates and Karan Lotfi, New England Medical Center, Boston, MA